

# Virtual Screening and Biological Evaluation of Potential PD-1/PD-L1 Immune Checkpoint Inhibitors as Anti-Hepatocellular Carcinoma Agents

Monica A. Kamal,<sup>†</sup> Hedy A. Badary,<sup>†</sup> Dalia Omran, Hend I. Shousha, Ashraf O. Abdelaziz, Hend M. El Tayebi,\* and Yasmine M. Mandour\*



Cite This: *ACS Omega* 2023, 8, 33242–33254



Read Online

ACCESS |



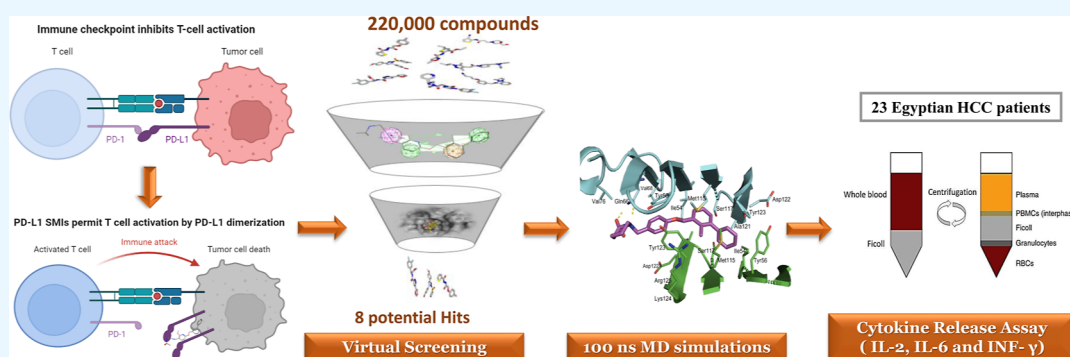
Metrics & More



Article Recommendations



Supporting Information



**ABSTRACT:** Blockade of the programmed cell death-1/programmed cell death ligand-1 (PD-1/PD-L1) immune checkpoint pathway is an efficient immunotherapeutic modality that provided significant advances in cancer treatment especially in solid tumors highly resistant to traditional therapy. Monoclonal antibodies (mAbs) and small-molecule inhibitors are the two main strategies used to block this axis with mAbs suffering from many limitations. Accordingly, the current alternative is the development of small-molecule PD-1/PD-L1 inhibitors. Here, we present a sequential virtual screening (VS) protocol involving pharmacophore screening followed by molecular docking for the discovery of novel PD-L1 inhibitors. The VS protocol resulted in the discovery of eight novel compounds. A 100 ns MD simulation showed two compounds, **H4** and **H6**, exhibiting a stable binding mode at the PD-L1 dimer interface. Upon evaluation of their immunological activities, the two compounds induced higher cytokines levels (IL-2, IL-6, and INF- $\gamma$ ) relative to BMS-202, 72 h post treatment of PBMCs of HCC patients. Thus, the discovered hits represent potential leads for the development of novel classes targeting the PD-L1 receptor as anti-hepatocellular carcinoma agents.

## 1. INTRODUCTION

Cancer immunotherapy represents a revolution in cancer treatment. Immunotherapy aims to improve the immune response toward cancer cells with few off-target effects which is a much-needed strategy for cancer treatment.<sup>1–3</sup> There are several classes of immunotherapies as cancer vaccines, oncolytic viruses, bispecific antibodies, immune system modulators, T-cell transfer therapy, and immune checkpoint inhibitors to name a few. The immune checkpoints act as brakes to the immune system to control excessive immune activation. The most investigated immune checkpoints are the cytotoxic T lymphocyte-associated molecule-4 (CTLA-4), programmed cell death receptor-1 (PD-1), and programmed cell death ligand-1 (PD-L1). PD-1 is expressed on the surface of activated T cells, and to preserve immunological homeostasis, these T-cells are momentarily inhibited upon binding of PD-1 with PD-L1.<sup>2</sup> Cancer cells frequently take advantage of this PD-1/PD-L1 binding as a way to escape the immune

system. In this context, it has been discovered that PD-L1 is overexpressed on the surface of several cancer types.<sup>4–8</sup> Therefore, in the tumor microenvironment, the upregulated PD-L1 binds to PD-1 and inhibits all the T cell-mediated anti-tumor immune responses, thus promoting the survival and growth of tumor cells.

A number of immune checkpoints inhibitors were approved by the FDA for patients with different types of cancer including melanoma, head and neck, lung, and bladder.<sup>8</sup> Moreover, some patients with various metastatic cancers have exhibited a significant survival advantage with the PD-1/PD-L1 check-

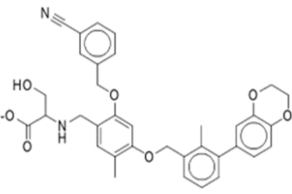
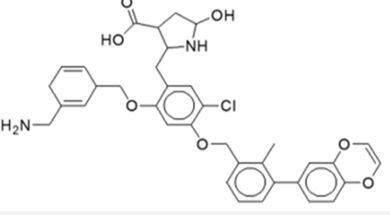
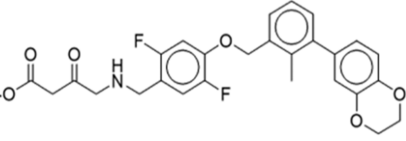
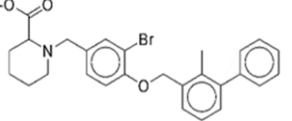
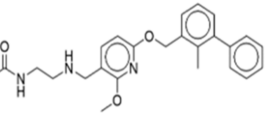
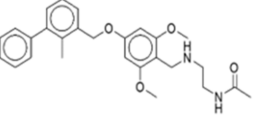
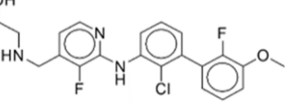
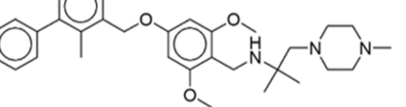
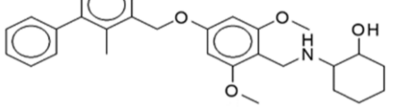
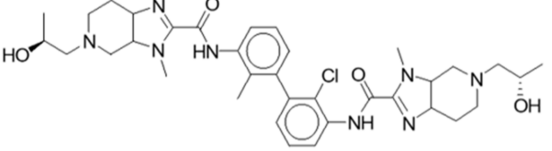
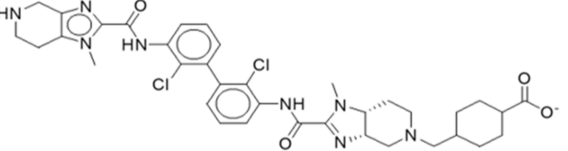
**Received:** January 17, 2023

**Accepted:** May 15, 2023

**Published:** September 3, 2023



Table 1. Chemical Structures of Training Set Compounds and their Reported IC<sub>50</sub> Values<sup>a</sup>

[3-(2,3-dihydro-1,4-benzodioxin-6-yl)-2-methylphenyl] methanol				
	Compound 1 (PDB: 5NIU) (IC <sub>50</sub> = 2.25 nM)	Compound 2 (PDB: 5NIX) (IC <sub>50</sub> = 1.4 nM)	Compound 3 (PDB: 5N2F) (IC <sub>50</sub> = 80 nM)	
	2-methyl-3-biphenyl methanol			
Compound 4 (PDB: 5J8O) (IC <sub>50</sub> = 146 nM)		Compound 5 (PDB: 5J89) (IC <sub>50</sub> = 18 nM)	Compound 6 (PDB: 5N2D) (IC <sub>50</sub> = 6-100 nM)	Compound 7 (IC <sub>50</sub> = 10-100 nM)
2-methyl-3-biphenyl methanol				
		Compound 8 (IC <sub>50</sub> < 10 nM)	Compound 9 (IC <sub>50</sub> = 6-100 nM)	Compound 10 (IC <sub>50</sub> = 6-100 nM)
	Tetra hydro imidazole [4,5c] pyridine			
Compound 11 (IC <sub>50</sub> < 10 nM)		Compound 12 (IC <sub>50</sub> < 10 nM)		

<sup>a</sup>Compounds are grouped based on their chemical scaffold.

point blockade.<sup>8,9</sup> Compared to PD-1, inhibition of PD-L1 appeared to be a more specific and efficient strategy with less severe side effects.<sup>10</sup> In recent years, anti-PD-L1 monoclonal antibodies have shown positive responses in clinical trials for a variety of malignancies. However, antibodies suffer from many limitations, such as the high production cost, low ability to penetrate the tumor tissues and immunogenicity to name a few, making small-molecule inhibitors (SMIs) an attractive alternative to inhibit PD-L1. Since 2016, several crystal structures for PD-L1 bound to SMI had been revealed.<sup>11-13</sup> The crystal structures showed these molecules to inhibit PD-1/PD-L1 binding by inducing PD-L1 dimerization, blocking its PD-1 interaction site. These crystal structures represent a valuable tool for structure-based design of PD-L1 inhibitors and thus can help in resolving the lag in the development of PD-L1 SMI. In this regard, Bristol-Myers Squibb (BMS) led a pioneering role in development of PD-L1 SMI in 2017. They reported derivatives of (2-methyl-3-biphenyl) methanol and [3-(2,3-dihydro-1,4-benzodioxin-6-yl)-2-methylphenyl] methanol with strong binding affinities to PD-L1, providing crystal structures for complexes of PD-L1 and inhibitors of these two classes.<sup>12</sup> Based on the latter, other research groups used the ring fusion strategy to synthesize benzo[*d*]isothiazole derivatives and quinazoline derivatives with strong inhibition of PD-1/PD-L1 interaction.<sup>14,15</sup> None of these molecules have been approved by FDA. However, several of these molecules are currently being tested in clinical trials.<sup>16,17</sup>

Aiming to find novel derivatives, in this study, we screened the commercially available SPECS<sup>18</sup> database to identify PD-L1 ligands. The virtual screening (VS) protocol was constructed based on the available crystal structures of PD-L1 protein along with structural information implied from previously reported PD-L1 inhibitors. Sequential screening using pharmacophore models and molecular docking was carried out on the database and promising hits were tested for their anti-hepatocellular carcinoma activity.

## 2. RESULTS

The crystal structures of PD-L1 complexed with several potent inhibitors (PDB code: 5J8O, 5J89, 5N2F, 5N2D, 5NIX, 5NIU)<sup>11-13</sup> were utilized to deduce the chemical characteristics of inhibitors' binding to the PD-L1 dimer. These crystal structures showed ligands centrally fitting at the interface of the PD-L1 homodimer interacting with both monomers. This channel-like binding site is mainly hydrophobic and could be subdivided into three regions: head (R1), central (R2), and tail (R3) regions.

**2.1. Pharmacophore Model Generation.** 3D pharmacophore models have proved to be a powerful tool in defining the essential chemical features for ligands' biological activity. In this work, a total of 12 previously reported PD-L1 inhibitors<sup>11-13,19</sup> characterized by their excellent experimental activities (Table 1), were used for building pharmacophore models for PD-L1 protein. The selected compounds were diverse in structure representing several chemical scaffolds: [3-

Table 2. Statistical Parameters of Pharmacophore Hypotheses Built with PD-L1 Training Set Compounds<sup>a</sup>

pharmacophore hypothesis	features	nA	TP %	sensitivity	nI	FP %	specificity	E.F.
PM-A1	Aro Hyd Hyd Don	84	95%	0.95	981	54%	0.46	1.8
PM-B1	Aro Aro Hyd Don	62	70%	0.70	167	9%	0.91	8.3

<sup>a</sup>nA: number of active hits. TP %: true positive percentage. nI: number of inactive hits. FP %: false positive percentage. EF: enrichment factor.

Table 3. Statistical Parameters of Refined Pharmacophore Hypotheses Built with PD-L1 Training Set Compounds<sup>a</sup>

pharmacophore hypothesis	features	radii	nA	TP %	sensitivity	nI	FP %	specificity	E.F.
PM-1	Aro Hyd Hyd Don	1 1.1 1.3 1.2	79	90%	0.9	709	39%	0.61	2.4
PM-2	Aro Aro Hyd Don Aro	1.3 1.3 1.3 1.5 2.3	62	70%	0.7	71	4%	0.96	14.4

<sup>a</sup>nA: number of active hits. TP %: true positive percentage. nI: number of inactive hits. FP %: false positive percentage. EF: enrichment factor.

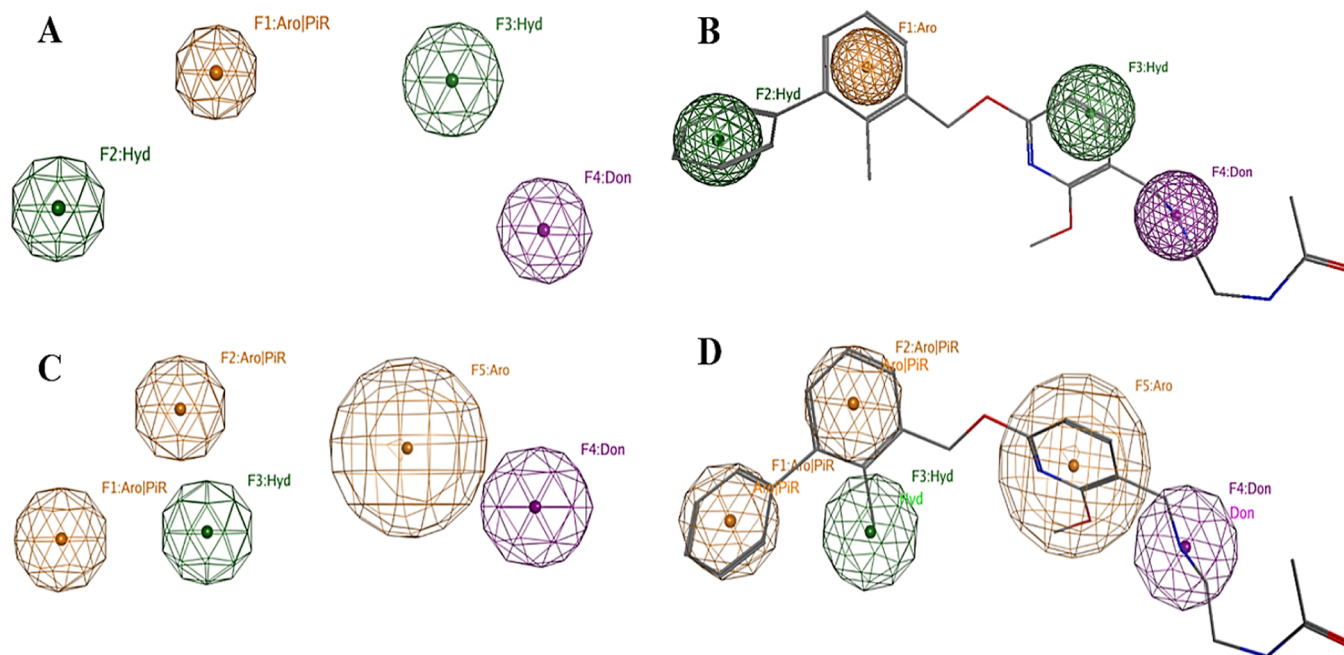


**Figure 1.** 3D spatial arrangement of (A) PM-1 and (C) PM-2 models. Mapping of compound 5 to the features of (B) PM-1 and (D) PM-2 models. The chemical features are represented as orange (aromatic, Aro), magenta (hydrogen bond donor, Don), and green (hydrophobic, Hyd) spheres.

(2, 3-dihydro-1, 4-benzodioxin-6-yl)-2-methylphenyl] methanol (compounds 1–3), 2-methyl-3-biphenyl-methanol (compounds 4–10) and tetra hydro imidazo [4,5C] pyridine (compounds 11 and 12). Two approaches were used to generate two sets of pharmacophore hypotheses. In approach A, we used the coordinates of compound 5 acquired from its crystal structure bound to PD-L1 dimer (PDB code: 5J89)<sup>11</sup> as a template to align the other 11 PD-L1 inhibitors using the align.svl script<sup>20</sup> available in Molecular Operating Environment

(MOE) version 2016.<sup>21</sup> Compound 5 was selected as it was of the highest affinity among the most common chemical scaffold (2-methyl-3-biphenyl methanol). In approach B, the coordinates of all six co-crystallized PD-L1 inhibitors (compounds 1–6) were used as a template to align the remaining six PD-L1 inhibitors. In either approach, low energy conformations were calculated for each compound, and the conformation showing the highest structural alignment to the template was chosen. The selected conformations were then used for constructing

pharmacophore models using the Pharmacophore Elucidate tool in MOE. Two resultant hypotheses, **PM-A1** and **PM-B1** from approaches 1 and 2, respectively, were found to comprise features matching the previously reported interactions for PD-L1 binding (Table 2). The active enrichment performance of these two models was then evaluated by retrospective screening.

Retrospective screening was used to assess the reliability of the selected models to distinguish between actives and inactives. Accordingly, a multi-conformation test set was built comprising 88 previously reported PD-L1 inhibitors<sup>22,23</sup> and 1821 compounds of similar physicochemical properties to PD-L1 inhibitors, labeled as actives and inactives with a ratio of 1:21; respectively. The inactive compounds comprised 11 previously reported molecules of poor affinity to PD-L1<sup>21</sup> along with 68 inhibitors of the cyclooxygenase-1 enzyme, angiotensin converting enzyme and beta-2 adrenergic receptor obtained from DEKOIS database,<sup>24</sup> three inhibitors of B7.1 (CD80) of the B7 family<sup>25</sup> and 1739 DUD-E generated decoys.<sup>26</sup> The models were evaluated based on the quantitative indicators, sensitivity, specificity, and enrichment factor (EF). As can be seen in Table 2, pharmacophore hypothesis **PM-A1** displayed very high sensitivity. Attempts were carried out to optimize the radii of the features to enhance the other two metrics: specificity and EF ending up with pharmacophore model **PM-1** in Table 3. **PM-1** comprised four features, an aromatic and a hydrophobic center representing R1, a hydrophobic center representing R2 and a hydrogen bond donor feature representing R3. **PM-1** was able to retrieve 79 out of 88 actives (sensitivity = 0.89), excluded 1112 out of 1821 inactive compounds (specificity = 0.61), and had a mapping EF of 2.4. On the other hand, the pharmacophore hypothesis **PM-B1** exhibited higher specificity and EF value (Table 3). However, it lacked the central hydrophobic feature representing R2. Accordingly, an aromatic feature, denoted as F5 in Figure 1D, was added to this hypothesis to increase its sensitivity leading to **PM-2**. **PM-2** comprised five features, a hydrophobic and two aromatic centers representing R1, an aromatic center representing R2, and a hydrogen bond donor feature representing R3. Upon retrospective screening, **PM-2** appeared more restrictive than **PM1**, retrieved 62 out of 88 actives (sensitivity = 0.7), excluded 1750 out of 1821 inactive compounds (specificity = 0.96), and showed an exceptionally high mapping EF of 14.4.

The two models contained features well representing the three main regions of the ligand binding pocket at the dimer interface. Mapping compound 5 on **PM-1** and **PM-2** (Figure 1) showed two identical features in both models: an aromatic feature representing the T-stacking interaction of the inner phenyl ring of the bi-aryl fragment with the side chain of TyrA56 in R1 and a hydrogen bond donor feature mapping the H-bond interaction of the ligand's nitrogen with the sidechain of AspA122 and LysA124 in R3. The hydrophobic interactions of the distal methyl phenyl ring of the bi-aryl fragment with AlaB121 and MetB115 in R1 were represented by either a hydrophobic or an aromatic center in models **PM-1** and **PM-2**, respectively. Similarly, the central phenyl ring with its interactions with the sidechain of TyrB56 and backbone atoms of AspA122 of R2 was represented by hydrophobic and aromatic centers in models **PM-1** and **PM-2**; respectively. Finally, **PM-2** comprised an extra hydrophobic center representing the methyl group on the distal methyl-phenyl ring fitting in R1. This methyl group was previously reported

to be crucial for achieving a non-coplanar configuration of the biaryl rings for optimal ligand fitting in the PD-L1 pocket.<sup>11,12</sup>

In conclusion, the shared chemical characteristics of the training set compounds served as a basis for the two constructed models (**PM-1** and **PM-2**) which contained features well representing the three main regions of the PD-L1 dimer interface. **PM-1** showed superiority with its high sensitivity (0.89); however, it had low specificity indicating that a considerable number of inactives were retrieved as well. Aiming to achieve balance between sensitivity and specificity as well as obtaining the greatest overall active enrichment, **PM-2** was constructed which showed dominance in specificity (0.96) compensating for **PM-1** in addition to a high EF of 14.4. In our VS protocol, we employed the concurrent usage of the two models to complement each other in their hit lists.

**2.2. Molecular Docking.** The next step in the VS protocol was molecular docking at the dimer interface of PD-L1 protein using GOLD 5.6 (Cambridge Crystallographic Data Centre, Cambridge, UK).<sup>27</sup> By the time of this study, seven crystal structures of the PD-L1 dimer co-crystallized with SMIs were published (5J8O, 5J89, 5N2F, 5N2D, 5NIX, 5NIU, and 6R3K).<sup>11–13</sup> Superimposition of the seven crystal structures showed high structural similarity with an average all-atom rmsd of 0.656 Å for all protein residues and 0.668 Å for the binding site residues. Accordingly, the crystal structure of PD-L1 dimer complexed with compound 4 crystal structure (PDB code: 5J8O)<sup>11</sup> was selected to be used in this study as it showed superiority in binding mode predictions (Table S1). To validate the ability of the docking protocol in pose predictions, the co-crystallized ligand 4 was docked into binding site at the junction of the two PD-L1 monomers. The resultant docked poses converged to a binding mode similar to the experimentally determined pose of compound 4 (Figure S1) with the best ranking pose showing an rmsd value of 1.124 Å (Table S2, Supporting Information). The binding pocket of PD-L1 homodimer is a deep hydrophobic channel-like pocket defined by residues of the 2 monomers and can be subdivided into three main regions as follows: head region (R1) defined by IleA54, ValA55, TyrA56, MetA115, IleA116, SerA117, MetB115, IleB116, SerB117, AlaB121, AspB122, and TyrB123, center region (R2) defined by AlaA121, AspA122, TyrA123, IleB54, ValB55, TyrB56, and GluB58, and the tail region (R3) defined by LysA124, ArgA125, GlnB66, ValB68, and ValB76. Compound 4 appeared completely occupying the dimeric interface extending from R1 to R3. The biaryl fragment occupied R1 with the distal phenyl ring involved with T-stacking interaction with the side chain of TyrA56 and hydrogen bond interaction with AspB122, while the second phenyl is involved with  $\pi$ -alkyl interactions with the side chains of MetA115 and hydrophobic interactions with IleA54 and MetB115. The central methyl phenyl ring and the piperidine ring fitted in R2 and R3, respectively. Given the exposed nature of R3, compound 4 exhibited several polar interactions in this region where the nitrogen of the piperidine ring was involved in hydrogen bond interaction with GlnB66 and the carboxylic group formed ionic interactions with LysA124.

Further evaluation of the docking protocol focused on how well it could distinguish between active and inactive compounds. To this end, docking of a test set comprising 50 actives and 1104 inactives was performed. GoldScore showed excellent enrichment performance with an AUROC value of 0.829 (Figure 2) and an EF at 1 and 5% of the ranked list of 17.32 and 8.36; respectively. It is worth mentioning that

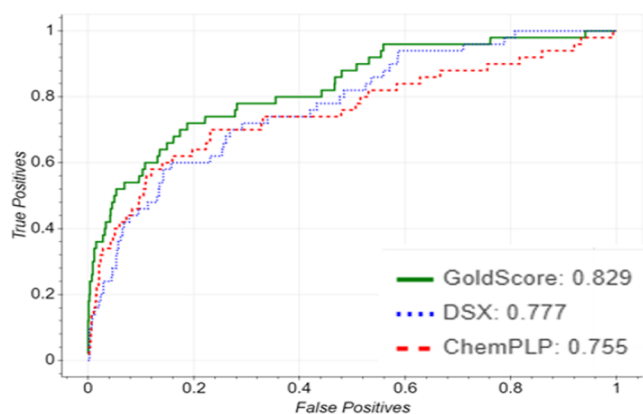


**Figure 2.** ROC curves obtained for the docked poses of validation database and plotted for various scoring functions: GoldScore (green solid curve), ChemPLP (red dashed curve), and DrugScore (blue dotted curve). Values of the areas under the curve (AUC) for each of the scoring functions is stated in the legend.

enrichment performance of the two other scoring functions: DSX<sup>PDB28</sup> and ChemPLP was assessed; however, GoldScore showed superiority, as shown by the AUROC and EF values (Figure 2 and Table 4).

**Table 4. Evaluation Metrics of the Three Scoring Functions: GoldScore, ChemPLP, and DrugScore<sup>a</sup>**

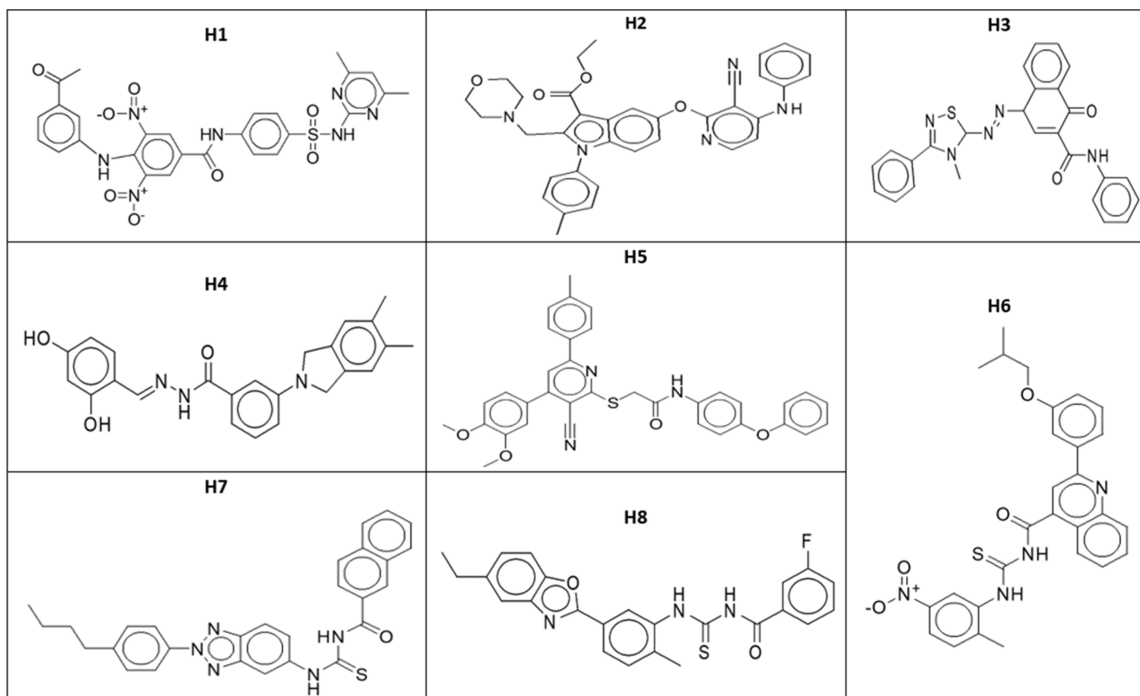
evaluation metric	E.F. <sub>1%</sub>	E.F. <sub>5%</sub>	AUROC
GoldScore	17.32	8.36	0.829
ChemPLP	9.7	6.7	0.777
DrugScore (DSX <sup>PDB</sup> )	9.67	4.81	0.755

<sup>a</sup>E.F.: enrichment factor. AUROC: area under the ROC curve.

**2.3. Prospective VS.** The two pharmacophore models PM-1 and PM-2 were used along with molecular docking to screen 211,235 compounds obtained from the SPECS database<sup>18</sup> for novel PD-L1 inhibitors. Specs database comprise compounds of drug-like properties, and thus, the database was directly uploaded in SMILES format to the Pharmit<sup>29</sup> server to undergo a knowledge-based conformational search. The resultant conformers were then mapped to the two pharmacophore models, PM-1 and PM-2. A total of 20,148 compounds matched PM-1, representing 6126 different chemical scaffolds, while only 719 compounds matched the more restrictive model, PM-2, representing 435 different chemical scaffolds. In total, the combined retrieval of the two pharmacophore models was 20,386 hits. The resultant hits of each pharmacophore model were separately docked into the dimeric interface of PD-L1 (PDB code: 5J8O<sup>11</sup>) using GOLD software<sup>27</sup> and the top 1% of the ranked compounds were selected. For PM-1 hits, 201 compounds represented the top 1% of the ranked list belonging to 127 different chemical scaffolds. For PM-2, seven compounds represented the top 1% of the ranked list belonging to five distinct chemical scaffolds. Given the high structural diversity among the top 1% compounds, due attention was given to the most populated chemical scaffolds where the best ranking molecule from each of these scaffolds was selected as a representative and visually examined. In total, 8 compounds (H1–H8) revealed promising binding modes to the PD-L1 receptor with the three compounds (H1, H2, and H5) matching the two pharmacophore models (Table 5).

**2.4. Biological Evaluation and Binding Mode Analysis.** **2.4.1. MTT Assay.** The cytotoxic effect of BMS-202 (compound 5) and compounds H1–H8 on Huh-7 cell viability was investigated in MTT dye reduction assay 48 h and 72 h post treatment with the compounds. All the compounds, including compound 5 as the positive control,

**Table 5. 2D Structures of the Virtual Screening Hits (H1–H8)**



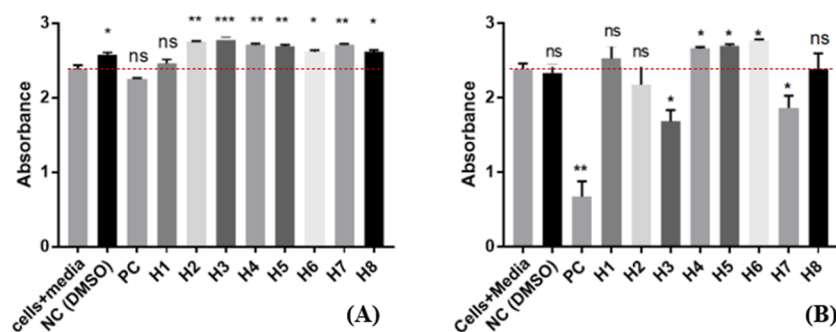


**Figure 3.** *In vitro* cytotoxic effect induced by compounds **H1–H8** post 48 h (A) and 72 h (B) treatment. The cytotoxicity levels were compared to the negative control using the unpaired *t*-test (\*\*\* =  $P < 0.001$ , \*\* =  $P < 0.01$ , \* =  $P < 0.05$ , ns: non-significant).

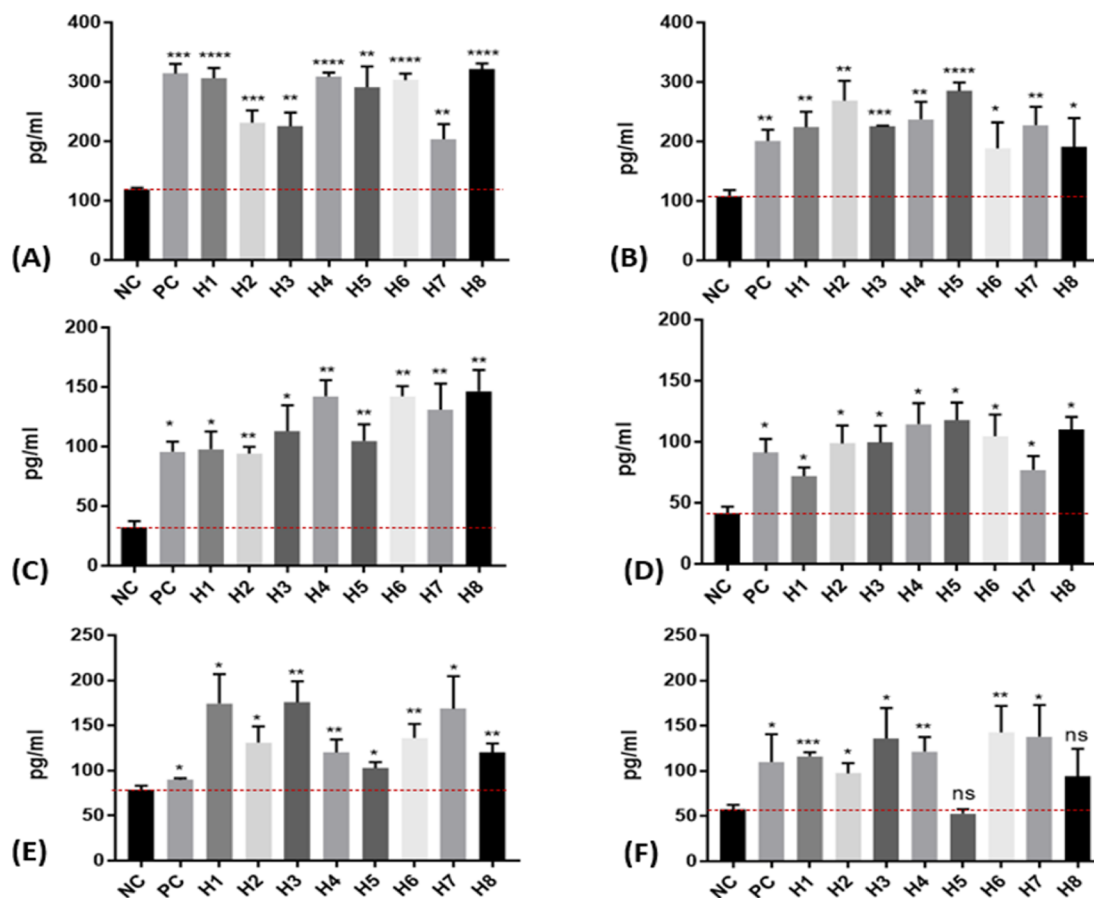


**Figure 4.** Levels of IL-2 (A,B), IL-6 (C,D), and INF- $\gamma$  (E,F) released by PBMCs of group A and B patients, respectively, 72 h. post-treatment with the hit compounds. NC: negative control. PC: positive control. Ns: non-significant. Every condition was done in triplicates.

showed very weak cytotoxic effects 48 h post-treatment (Figure 3A). Interestingly, 72 h post-treatment, compound **5** showed a threefold decrease in the number of viable cells. On the other hand, compounds **H1**, **H2**, **H4**, **H6**, and **H8** showed no cytotoxic effects 72 h post-treatment with only compounds **H3** and **H7** showed a onefold decrease in the number of viable cells. These results indicate that compounds **H1**, **H2**, **H4**, **H6**, and **H8** were non-toxic to cells while only mild cytotoxic effects were observed 72 h post-treatment with compounds **H3** and **H7**.

**2.4.2. IL-2, IL-6, and INF- $\gamma$  ELISA Assay.** Measuring the compounds' induced cytokines release in the tumor micro-environment is an indicator of their effect on the activity of PBMCs. Accordingly, the effects of BMS-202 (compound **5**)

and compounds **H1–H8** on the levels of interleukin-2 (IL-2), interleukin-6 (IL-6), and interferon-gamma (INF- $\gamma$ ), were analyzed in the supernatants of the co-cultured hepatocellular carcinoma (Huh-7 cells) with PBMCs 72 h post-treatment with the compounds. The PBMCs were isolated from the blood of HCC patients categorized by Child-Pugh score system into A and B groups. Five clinical indicators of liver disease and the potential for eventual liver failure are scored to determine the Child-Pugh score. Each metric is given a score of 1, 2, or 3, with 3 being the most severe. These five indicators are as follows: total bilirubin, serum albumin, prothrombin time or INR, ascites, and hepatic encephalopathy. The calculation of the Child-Pugh score is similar to using a calculator. It is determined by adding together the score of the five items.

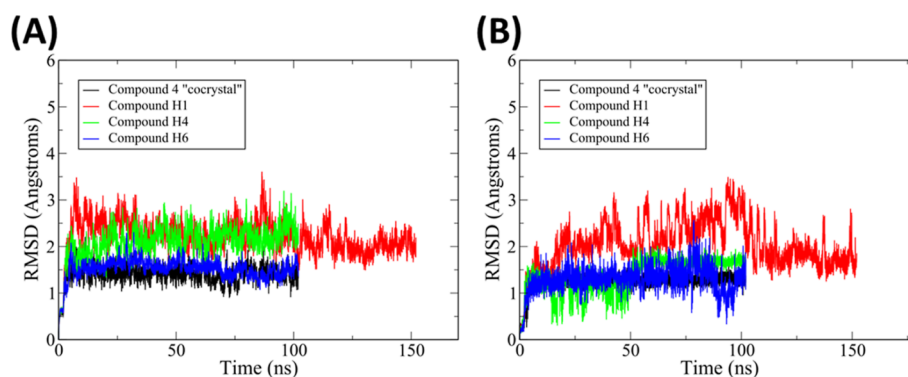


**Figure 5.** Time evolution of root-mean-square deviations of the entire trajectory consisting of structures sampled in intervals of 20 ps. The plot depicts rmsd values based on (A) protein backbone atoms excluding the termini and (B) ligand heavy between the trajectory frames and the starting geometry.

**Table 6. H-Bond Analysis of the 100 ns of the MD Trajectory of Compounds H1, H4, and H6<sup>a</sup>**

HB-acceptor	HB-donor	donor	persistence percentage along the MD trajectory	average H-bond distance (Å)	average H-bond angle
Compound <b>H1</b>					
LIG_248@O4	GLN_B66@HE21	GLN_B66@NE2	42%	2.87	159.9
LIG_248@O3	ASN_B63@HD21	ASN_B63@ND2	20%	2.84	153.9
Compound <b>H4</b>					
GLN_B66@OE1	LIG_248@H26	LIG_248@N26	28%	2.87	144.2
Compound <b>H6</b>					
ASP_A122@OD2	LIG_248@H3	LIG_248@N3	57%	2.80	155.2
ASP_A122@OD2	LIG_248@H2	LIG_248@N2	55%	2.80	152.4
ASP_A122@OD1	LIG_248@H3	LIG_248@N3	32%	2.80	155.2
ASP_A122@OD1	LIG_248@H2	LIG_248@N2	32%	2.80	152.6
LIG_248@O7	GLN_B66@HE21	GLN_B66@NE2	18%	2.86	155.5
LIG_248@O7	GLN_B66@HE22	GLN_B66@NE2	14%	2.83	153.7
Control					
GLN_B66@OE1	LIG_248@H	LIG_248@N	94%	2.80	163.6
LIG_248@O2	GLN_B66@HE21	GLN_B66@NE2	41%	2.84	165.3
LIG_248@O1	GLN_B66@HE21	GLN_B66@NE2	38%	2.84	165.2

<sup>a</sup>Only H-bonds that are persistent in more than 10% of the snapshots are included. For each H-bond, column 1 represents the acceptor residue and atom name. Columns 2 and 3 indicate the name of the H-atom and the electronegative atom attached to it on the donor residue, respectively.

Patients who score 5 to 6 points are categorized as Child-Pugh A and they have the least severe liver disease with 95% chance of 1 to 5-year survival rate. On the other hand, patients who score 7 to 9 points are categorized as Child-Pugh B and they have moderately severe liver disease with 75% chance of one to five-year survival rate. The cytokine levels were detected using enzyme linked immunosorbent assay (ELISA).

All the compounds have shown significant increase in the levels of the three cytokines, IL-2, IL-6, and INF- $\gamma$  in the two clinical stages (Figure 4). The ability of the compounds to induce IL-2 and IL-6 appears dependent on the patient's clinical stage where higher levels of the two cytokines were observed in group A relative to group B patients. This appeared less obvious for INF- $\gamma$ , where relatively similar levels were observed in the two patient groups. The three compounds **H1**, **H4**, and **H6** showed consistent increase in the levels of the three cytokines relative to the positive control (PC), compound 5. The level of IL-2 induced by compounds **H1**, **H4**, and **H6** was roughly 300 pg/mL for all three compounds, versus 310 pg/mL for the PC in group A patients. However, IL-2 levels for group B patients were 215 pg/mL, 220 pg/mL, and 185 pg/mL for compounds **H1**, **H4**, and **H6**, respectively compared to 200 pg/mL for the PC. The level of

IL-6 for compound **H1** was 100 pg/mL, while compounds **H4** and **H6** induced the same level of 140 pg/mL in comparison to 95 pg/mL for the PC for group A patients. In group B patients, compounds **H1**, **H4**, and **H6** induced different levels of IL-6: 70, 120, and 105 pg/mL, respectively, in comparison to 80 pg/mL for the PC. The levels of INF- $\gamma$  for compounds **H1**, **H4**, and **H6** were 175 pg/mL, 120 pg/mL, and 140 pg/mL, respectively, in comparison to 90 pg/mL for the PC for group A patients while 120, 125, and 145 pg/mL, respectively, in comparison to 110 pg/mL for the PC in B group patients.

**2.5. In Silico Binding Mode Analysis.** The three compounds **H1**, **H4**, and **H6** showed consistent increase in cytokines' levels in the functional ELISA assays and thus, their binding modes to the PD-L1 receptor were further investigated. Compound **H1** was retrieved by both models **PM-1** and **PM-2**, while **H4** and **H6** were retrieved by **PM-2** and **PM-1**, respectively. For these three compounds, the stability of their docked poses was checked by carrying out a 100 ns molecular dynamics simulation using the AMBER software package.<sup>38</sup> For comparison, a 100 ns MD simulation was also carried out for the experimentally determined X-ray structure of PDL-1 complexed with compound 4 (PDB code: 5J8O<sup>11</sup>). Visual examination of the resultant trajectories

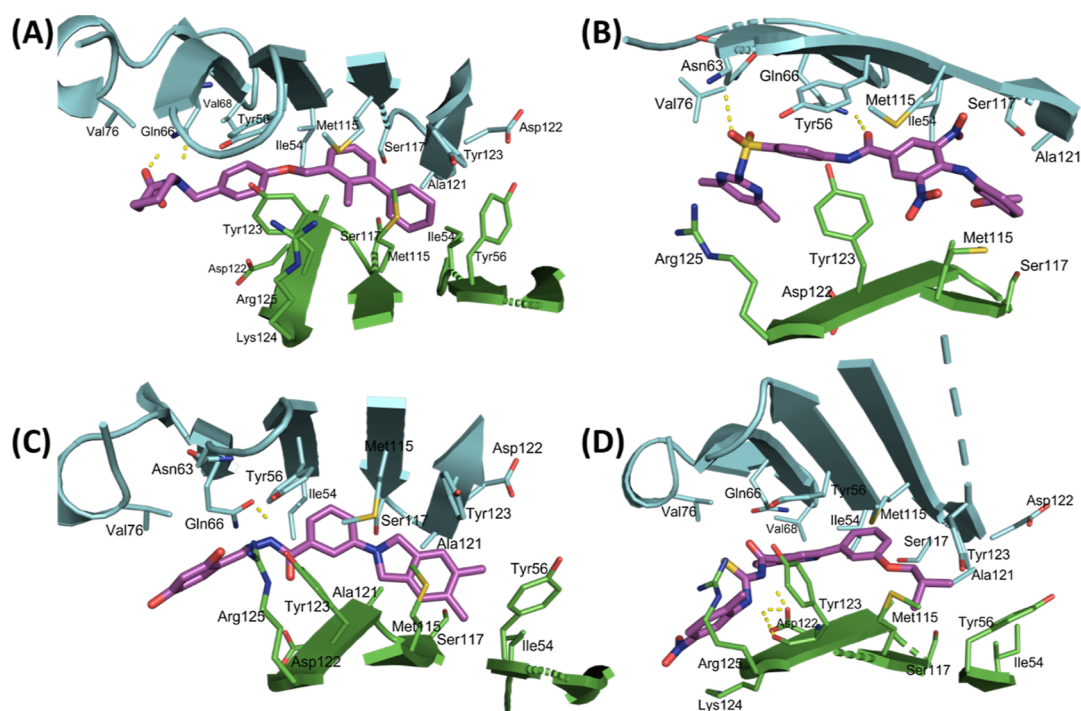


**Figure 6.** Binding mode of the hit compounds at the PD-L1 dimer interface. A representative MD structure of PD-L1 bound to the docked pose of (A) compound 4, (B) H1, (C) H4, and (D) H6. PD-L1 chains A and B are depicted as green and cyan cartoon; respectively. The cocrystallized compound 4 was added for comparison.

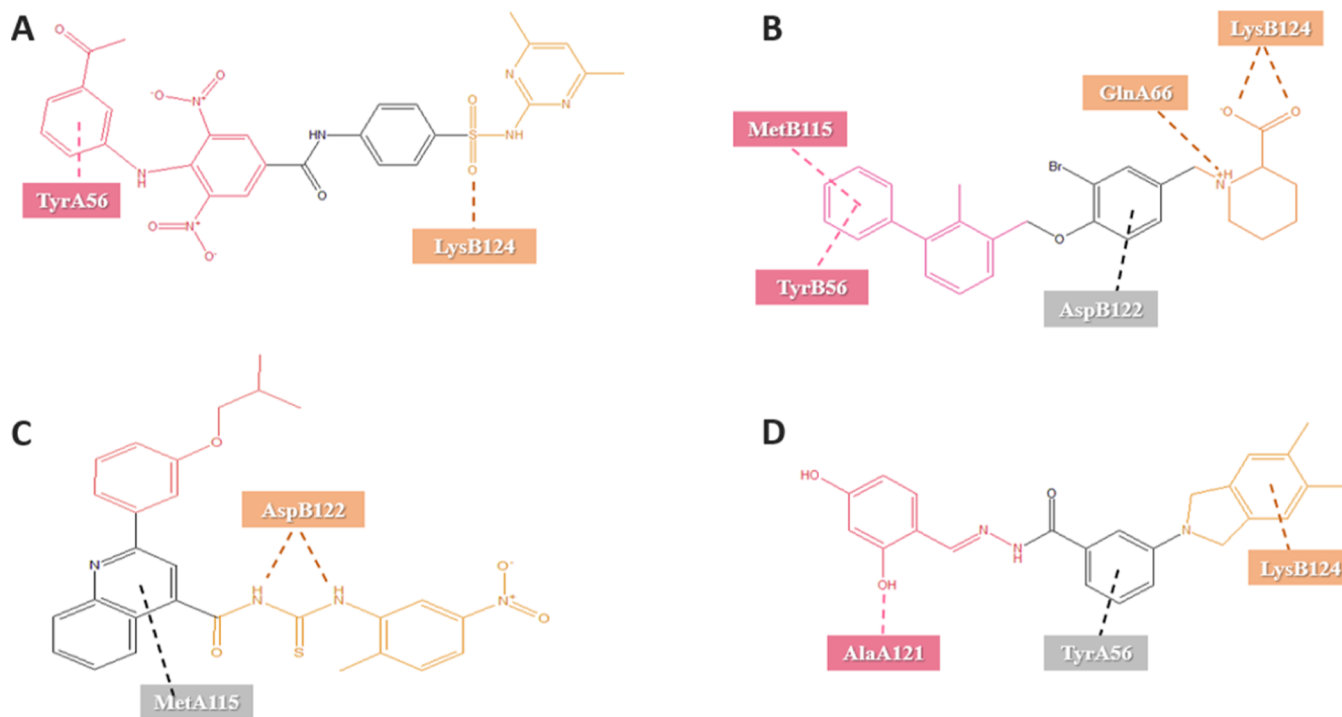


**Figure 7.** Chemical structures of hit compounds (A) H1, (B) compound 4, (C) H6, and (D) H4 showing the parts fitting in R1 (orange), R2 (gray), and R3 (red) regions of the binding pocket at PD-L1 dimer interface. Interactions between the ligands and specific PD-L1 residues are depicted by dotted lines. Structure of the co-crystallized compound 4 is added for comparison.

showed the three compounds maintaining their initial docked poses at the PD-L1 dimer interface. rmsd analysis of the ligand non-hydrogen atoms showed less than 2 Å deviations from the initial docked pose for compounds H4 and H6 in analogy to 4 (Figure 5). Similarly, a plateau was observed for the rmsd fluctuations of the protein backbone atoms after 20 ns.

However, compound H1 showed larger fluctuations and thus the simulation was extended for an additional 50 ns, where it seemed to maintain a stable binding mode (Figure 5B).

H-bond analysis was performed on the stable part of the production MD trajectories with frames sampled every 10 ps for the last 60 ns. As shown in Table 6, all H-bonds were



mainly found in the polar R3 tail region, in agreement with the H-bond donor feature in the proposed pharmacophore models (PM-1 and PM-2). Compound 4 showed an exceptionally persistent H-bond with the sidechain of GlnB66 which was maintained in 94% of the sampled frames. Interestingly, the three compounds H1, H4, and H6 showed the same H-bond interaction with GlnB66 maintained in 42, 28, and 19% of the sampled frames, respectively.

For each hit compound, an average structure of the collected snapshots for the last 60 ns was generated, and the MD snapshot with the highest structural similarity with this average structure was chosen to examine the binding modes of these hits. The three compounds appeared to bind to PD-L1 in a similar orientation to that of compound 4, occupying the three main regions of the channel-like pocket (Figures 6 and 7). Compound H1 had its dinitrobenzene occupying R1 with its 4-phenyl ring forming arene-H interaction with AlaA121, its central phenyl amide fitted in the central R2 region with its amide oxygen forming H-bond with the sidechain of GlnB66 of R3 which is maintained in 42% of the trajectory frames, while the pyrimidine ring fitted in R3 with its sulfamoyl group forming strong H-bonds with AsnB63 of R3 that are maintained in 20% of the trajectory frames. Compound H4 showed its 1,3-dihydro-2H-isoindol-2-yl group occupying R1 and forming arene-H interactions with AlaA121 and MetA115, its hydrazine group fitting in R2 and forming a H-bond with the side chain of GlnB66, while its di-hydroxybenzylidene group fitting in Rb3. Compound H6 showed its 3-isobutoxy phenyl group fitting in R1 region, the isoquinoline ring occupying R2 region, while the polar thiourea group extending in R3 with its two nitrogen atoms involved in the H-bond interaction with AspA122 maintained in more than 50% of the sampled frames, while the adjacent carbonyl formed a H-bond interaction with the side chain of GlnB66 maintained in at least 18% of the sampled frames. It is worth mentioning that the largest variations in the compounds structures was in the fragments fitting in the tail R3 region.

Finally, MM-GBSA method was used to compare the binding affinities of these three hit compounds to that of compound 4. The binding free energy of each hit-PD-L1 complex was calculated by sampling frames at a regular interval of 10 ps from the last 60 ns trajectory for the MM-GBSA calculations (Table 7). Compound H4, displayed a relatively

**Table 7. List of MM-GBSA Binding Free Energies (in kcal/mol) for Compounds H1, H4, H6, and Cocrystallized Compound 4 Bound to PD-L1 Protein**

compound	MMGBSA (kcal/mol)	std deviation	std. error of mean
compound H1	-36.8120	4.6452	0.0848
compound H4	-42.4763	2.7283	0.0610
compound H6	-54.8842	3.9636	0.0724
compound 4	-43.6884	7.4679	0.1363

similar binding affinity score to that of the co-crystallized compound 4 of -42.5, and -43.7 kcal/mol, respectively, while compound H6 showed significantly higher binding affinity of -54.9 kcal/mol. The relative binding affinities of the compounds confirmed the superiority of compound H6 in accordance with the results of the H-bond analysis.

### 3. DISCUSSION

PD-1/L1 immune checkpoint inhibitors have become the emerging core of tumor treatment because of their potential effectiveness. Disrupting the PD-L1-mediated tumor immune escape by SMIs is more advantageous over monoclonal antibodies (mAbs). Despite their positive therapeutic efficacy, mAbs suffer from many limitations such as immune-related side effects (irAEs), complex production process, high treatment costs, and low permeability in the tumor tissues.<sup>30-32</sup> On the other hand, SMIs have better oral bioavailability and tumor penetration, easier self-administration and have fewer side effects compared to mAbs,<sup>30</sup> making immunomodulation by SMI an attractive approach for cancer treatment as reviewed.<sup>33</sup> The increasing number of available crystal structures for PD-L1 bound to inhibitors helped in understanding the mechanism of inhibition of these compounds and paved the way for discovery of novel PD-L1 inhibitors.<sup>11,15</sup>

In this study, the 3D crystal structure of human PD-L1 protein complexed with a SMI was used to design a sequential VS protocol comprising pharmacophore screening followed by molecular docking. SMIs bind at the PD-L1 dimer interface in a tunnel-like binding pocket that can be divided into head (R1), center (R2), and tail (R3) regions. The pharmacophore models comprised four main features distributed within the tunnel as follows: (a) an aromatic center for T-stacking interaction with the side chain of TyrA56 in the head region, R1. (b) A hydrophobic center for interactions with AlaA121 and MetB115 in R1, (c) an aromatic center for interaction with TyrB56 and backbone of AspA122 at the tunnel's central region, R2, and (d) a hydrogen bond donor feature representing interactions with residues at the polar exposed tail region, R3. Applying the VS protocol on the commercially available SPECS database recognized eight compounds with promising binding modes mimicking those of previously crystallized PD-L1 inhibitors, suggesting a similar PD-L1 dimer locking inhibition mechanism for these compounds.

The compounds' effect on HCC was evaluated by checking the levels of the three cytokines, IL-2, IL-6, and INF- $\gamma$ , upon the treatment of PBMCs of HCC patients with each compound. The cytokines levels have been reported as biomarkers of the patient's response to monoclonal antibodies, immune checkpoint inhibitors and the accompanying immune related adverse events as well.<sup>34,35</sup> All the tested compounds have shown an increase in the levels of IL-2, IL-6, and INF- $\gamma$  in the two patients' clinical stages. The ability of the compounds to induce IL-2 and IL-6 appears dependent on the patient's clinical stage where higher levels of the two cytokines were observed in group A relative to group B patients. This appeared less obvious for INF- $\gamma$ , where relatively similar levels were observed in the two patient groups. For IL-2, H1, H4, H6, and H8 showed comparable levels to the PC in group A and B patients, while H1 and H4 induced 1.1- and 1.15-folds higher levels than the PC in group B patients; respectively. For IL-6, both H4, H6, and H8 exhibited 1.47-, 1.47-, and 3.6-folds higher levels than PC in group A patients, whereas 1.5-, 1.3-, and 2.5-folds higher levels than PC in group B patients, respectively. For INF- $\gamma$ , H1, H4, and H6 showed 1.9-, 1.3-, and 1.5-folds higher levels than the PC in group A patients. For group B patients, H4 and H6 induced 1.1- and 1.3-folds higher levels of INF- $\gamma$  than the PC with H1 inducing the same amount as PC. Altogether, compounds H1, H4, and H6 have

induced an increase in the levels of the three cytokines in a comparable or even superior manner to the PC with the highest increase observed in the levels of IL-2.

MD simulation of these three promising compounds showed compounds **H4** and **H6** to exhibit a stable binding mode at the PD-L1 dimer interface similar to PD-L1 cocrystallized ligands. H-bond analysis showed the three ligands acting as H-bond donors, maintaining a stable H-bond interaction in R3 region in agreement with the results of the pharmacophore models. Additionally, the sidechain of GlnB66 showed a persistent interaction with the compounds throughout the simulation, indicating this residue to be crucial for maintaining a stable binding mode for the compounds at the PD-L1 dimer interface. Together, the results of MD simulation and pharmacophore models suggest the importance of hydrophobic/aromatic interactions at the head R1 region and a H-bond donor feature in the tail R3 region.

The stable binding mode of **H4** and **H6** compounds was further confirmed by free energy calculations which showed the two compounds to exhibit a similar or even superior binding affinities to PD-L1 relative to that of the cocrystallized compound **4**, respectively. This suggests that the observed increase in cytokines levels upon treatment with compounds **H4** and **H6** is a result of PD-L1 binding. However, homogeneous time resolved fluorescence assay is still required to confirm PD-L1 binding of these two compounds.

In conclusion, a sequential multi-stage VS protocol was applied on the commercially available SPECS database to find novel PD-L1 inhibitors, identifying eight promising compounds of novel chemical scaffolds. Two compounds showed ability to induce higher levels of IL-2, IL-6, and INF- $\gamma$  relative to BMS-202 upon treatment of PBMCs of HCC patients. MD simulations showed a stable binding mode for these two compounds at the PD-L1 dimer interface. These two compounds, **H4** and **H6**, represent promising leads for targeting PD-L1 receptor as anti-hepatocellular carcinoma agents.

## 4. METHODOLOGY

**4.1. Compound Preparation.** Using Molecular Operating Environment (MOE) version 2016 software,<sup>21</sup> all the molecules in the databases were prepared by washing, partial charge calculation, and energy minimization utilizing MMFF94x forcefield and 0.0001 kcal/mol as a gradient. The low MD conformational search algorithm was implemented in MOE and produced multiple conformations of compounds using the following parameters: energy window (7 kcal/mol), rejection limit (10,000 steps), minimization (MM) iteration limit (10,000 steps), elimination of the duplicate conformer threshold (rmsd, 0.005), total number of iterations (10,000 steps), and maximum conformation limit (10,000 conformers).

**4.2. Pharmacophore Model Generation.** 12 known PD-L1 inhibitors in total, distinguished by their exceptional experimental performances, were gathered from literature, and used as a training set for building the pharmacophore model. For constructing **PM-1**, using MOE's align.svl script, which is openly available, the training set compounds were aligned on the experimentally determined coordinates of compound **5**. For each compound, a series of alignments was calculated through a stochastic conformational search with a 7 kcal/mol energy window. Using MOE's Pharmacophore Elucidate module, it was decided to start with the conformation that had the most negative F score and the highest resemblance to

compound **5** in order to find the common pharmacophoric features between all active compounds in the training set. For constructing **PM-2**, bioactive conformations of compounds (**1–6**) representing the co-crystallized ligands of the published PD-L1 dimer crystal structures were overlaid using the script (align.svl). This overlay was then used as a template for aligning the rest of the training set compounds (**7–12**). Based on the unified annotation scheme, pharmacophore features and projected pharmacophore features were used to create the pharmacophore models. Models were generated automatically so that the generated queries had a maximum of five features and matched all compounds in the training set. The smallest permitted distance between features was set at 1.0 Å, and features were clustered together if they were more than 1.25 Å apart. The resulting pharmacophore hypotheses were verified using a test set comprised of 88 previously reported PD-L1 inhibitors, which were labelled as actives. The inactive test set compounds included 12 PD-L1 inhibitors of low activity, 69 inhibitors of cyclooxygenase-1 enzyme, angiotensin converting enzyme and beta-2 adrenergic receptor obtained from DEKOIS<sup>24</sup> database, three inhibitors of B7.1 (CD80) of the B7 family, along with 1876 decoys generated by generated by Directory of Useful Decoys<sup>26</sup> (DUD-E). The database was prepared as mentioned in the compounds preparation (Section 4.1). The test set molecules were mapped to the two pharmacophore models; **PM-1** and **PM-2**; using MOE and the quality of the models was decided based on the statistical metrics: selectivity, specificity, and EF values.

**4.3. Molecular Docking.** GOLD<sup>27</sup> (version 5.6) was used to conduct the molecular docking experiments using the crystal structure of PD-L1 receptor complexed with the potent SMI **4** (PDB: 5J8O).<sup>11</sup> Active site residues were specified by the crystal coordinates of compound **4** and utilizing the default cutoff radius of 6 Å, with the “detect cavity” option enabled. The docking experiments were performed using the GoldScore scoring function. The search efficiency of the algorithm was set at 200% setting with a rigid receptor with the 50 resultant poses clustered based on their rmsd as previously described.<sup>36</sup> The efficiency of pose prediction was evaluated using the heavy atom rmsd between the docked poses and the experimental coordinates of compound **4**. Retrospective screening of a test set database of 1154 compounds was used to evaluate the enrichment performance of the docking protocol. The test set included 50 PD-L1 inhibitors obtained from literature along with 1104 inactive compounds. Different scoring methods were evaluated where the true positive rates and false positive rates were used to plot the receiver operator characteristic (ROC) curve. For prospective VS runs, the EF and area under the ROC curve (AUROC) values were computed to select the best scoring method. Figures were prepared using Pymol.<sup>37</sup>

**4.4. Prospective VS.** The commercially available Specs<sup>18</sup> database was screened using the 3D queries: **PM-1** and **PM-2**. Compounds were prepared in accordance with compound preparation (Section 4.1) and saved in SMILES file format. Then, 3D conformations were generated using Pharmit server and its knowledge-based conformational search algorithm.<sup>29</sup> The resulting conformations were mapped to the pharmacophore models such that hits were counted if they matched every feature of the query. Next, GoldScore scoring function was employed to dock the identified hits into the ligand's binding pocket at PD-L1 dimer interface using GOLD<sup>27</sup> software. The genetic algorithm's search efficiency was set at 200%, while the receptor was retained rigid.

**4.5. Molecular Dynamics.** For the complexes of PDL-1 with each of compound **H1**, **H4**, and **H6**, MD simulations were carried out using the PMEMD.cuda code of the AMBER Molecular Dynamics package<sup>38</sup> following the same previously described protocol of minimization, heating, density equilibration, and production.<sup>39,40</sup> The trajectory lengths for heating, density equilibration, and production were 20 ps, 200 ps, and 100 ns, respectively. The trajectories were analyzed using CPPTraj.<sup>41</sup> Plots and visual inspection of the trajectories was done using XMGrace<sup>42</sup> and VMD,<sup>43</sup> respectively.

Two minimization cycles were conducted on each complex to remove bad contacts. In the first minimization run, strong restraints were applied on the non-solvent residues, with a force constant of 500 kcal/mol. Å<sup>2</sup>. The system was then heated from 0 K to 300 K using the Langevin thermostat. Density equilibration and production were conducted at constant pressure (1 atm). Langevin dynamics<sup>44</sup> were generally employed and the Particle-Mesh Ewald method<sup>45</sup> was used to treat long-range electrostatics under periodic boundary conditions.

**4.6. Free Energy Calculations.** Following the MD simulation, for each complex, the last 10 ns of the MD trajectory was used to compute the binding free energy. For this purpose, we employed the MM-GBSA method. The snapshots were sampled at a regular interval of 10 ps and thus a total of 1000 frames were used to calculate the MM-GBSA energies.<sup>46</sup> All MM-GBSA calculations in this study were carried out using the MMPBSA.py script included in AmberTools.<sup>38</sup>

**4.7. Subjects and PBMCs Isolation from Whole Blood.** Approximately 8 mL of fresh peripheral venous blood were withdrawn from 13 HCC patients (7 patients; child score A and 6 patients; child score B), who were enrolled from the multidisciplinary HCC clinic, Cairo university, upon their written consent\*. The blood was collected in EDTA tubes to prevent coagulation. Within 3 or 4 h of sample collection, the Ficoll separation technique was applied to isolate the PBMCs from the whole blood. For each sample, each 3 mL of fresh venous blood was diluted in a ratio of 1:1 using wash mix [94 mL of RPMI supplemented with L-glutamine + 5 mL of FBS (biowest) + 1 mL of Penicillin/Streptomycin (ThermoFisher)]. Using a sterile Pasteur pipette, each 6 mL of the diluted blood was layered carefully onto 3 mL of Ficoll hydrate (GE Healthcare). Blood is separated into three layers after centrifugation at 4000 rpm for 30 min with no brakes. Next, the middle buffy layer, including the PBMCs, was carefully gathered and washed by wash mix three consecutive times to remove any contaminating platelets. Then, a check for cell viability and an approximation of PBMCs count were assessed using trypan blue where viable cells were counted in a Neubauer counting chamber. Finally, PBMCs of each patient were cryo-preserved and stored in the -80 °C for later use.

**4.8. Cell Line.** Huh-7, human liver cell line obtained from Vacsera. It was cultured in Full DMEM culture medium (Biowest) and maintained to be ready for assessing the antineoplastic activity of the purchased compounds. The cell line was nurtured under incubation standard conditions (37 °C and 5% CO<sub>2</sub>) with a humidified atmosphere. The sterile Huh-7 cell line are passaged consistently to maintain the logarithmic growth phase of the cell population.

**4.9. Compounds' Stock Solutions Preparation.** The stock solutions of the purchased compounds were prepared using DMSO (LOBA chemie) as a solvent. Compounds (**H1**,

**H2**, **H3**, **H4**, **H6**, **H7**, and **BMS-202**) were prepared in a stock solution of 4 mg/mL. Compounds **H5** and **H8** were prepared in a stock solution of 1 mg/mL due to their low solubility in DMSO. All the stocks were kept in sterile Eppendorf tubes and stored at -20 °C.

**4.10. Statistical Analysis.** GraphPad Prism 7.04 was used to conduct the analysis, and the data were represented as the mean ± standard error of the mean (SEM). A *P*-value of 0.05 or lower was regarded as statistically significant. One-way ANNOVA and the unpaired *t*-test were used to statistically validate the tests that were run (\*\*\*\* = *P* value less than 0.0001, \*\*\* = *P* value less than 0.001, \*\* = *P* value less than 0.01, and \* = *P* less than 0.05).

**4.11. MTT Assay.** The viability of Huh-7 cells was assessed by MTT (3-[4, 5-dimethylthiazol-2-yl]-2, 5 diphenyl tetrazolium bromide) dye reduction assay after treatment with compounds (**1–8**) and **BMS-202** (MedChemExpress) as a positive control, keeping the control untreated cells subjected to the same conditions excluding the treatment by the compounds. Briefly, 96-well plates were used to seed the Huh-7 cells and then treated with 50 μM of compounds. This dose was selected according to the previously reported cytotoxic doses in literature for similar compounds to ours (**BMS-103** and **BMS-142**) on HepG2 cell line.<sup>2</sup> After 48 and 72 h from the treatment, 200 μL of MTT working solution (5 mg/mL in PBS) is added to the surviving cell fractions and dissolving newly formed formazan crystals with 100 μL of lysis solution (DMSO + 96% ethanol) in the control and treated groups (three replicates/sample). Using the plate reader victor 1420 (PerkinElmer, USA), the absorbance was measured at 595 nm wavelength. Cell survival rates were calculated as the percentages of untreated controls and determined by GraphPad Prism 7.04 software.

**4.12. Coculture of PBMCs with Compounds and Huh-7 Cell Line.** Concisely, isolated PBMCs from group A and B HCC patients were thawed in room temperature and then quickly added to 6 mL of warm wash mix [94 mL of RPMI supplemented with L-glutamine + 5 mL of FBS (biowest) + 1 mL of Penicillin/Streptomycin (ThermoFisher)]. Pellets were collected by centrifuging at 1600 rpm for 5 min. The supernatants were discarded and the PBMCs were re-suspended in full RPMI medium (biowest). Then, PBMCs were activated by 0.5% (v/v) phytohemagglutinin for 48 h and co-cultured on previously seeded Huh-7 cells and treated with 50 μM of compounds for 72 h. Each condition was done in triplicates.

**4.13. Cytokine Release Assay.** Sandwich ELISA kit (My BioSource) was used. 0.1 mL of 1000, 500, 250, 125, 62.5, 31.2, and 15.6 pg/mL standard solutions into the standard wells. This was followed by the addition of 0.1 mL of each sample over the standard diluent buffer into the control and test sample wells and incubated at 37 °C for 90 min with each sample done in triplicates. The plate content was discarded and clapped on an absorbent material to remove the unbound antigen. Then, 0.1 mL of biotin conjugated anti-Human (IL-2/INF-γ/IL-6) antibody work solution was added into the above wells (standard, test sample, and control wells). The plate was covered and incubated at 37 °C for an hour. The solutions in the plate were discarded and clapped on absorbent material. Each well was filled with Wash buffer and vortexed gently on ELISA shaker for 2 min, and then, contents were aspirated from the plate. Finally, the plate was clapped on absorbent material. This procedure was repeated two more times for a

total of three washes. 0.1 mL of ABC working solution was added into each well. The plate was covered and incubated at 37 °C for 30 min and washed five times. 90 μL of TMB substrate was added into each well. The plate was covered and incubated at 37 °C in the dark for 15–20 min. 0.1 mL of stop solution into each well was added and mixed. The color changes into yellow immediately. Then, absorbance was measured at 450 nm in a microplate reader within 30 min after adding the stop solution. The density of color is proportional to the (IL-2/INF-γ/IL-6) amount of sample, and then, the concentrations of (IL-2/INF-γ/IL-6) were calculated using a calibration curve.

## ■ ASSOCIATED CONTENT

### SI Supporting Information

The Supporting Information is available free of charge at <https://pubs.acs.org/doi/10.1021/acsomega.3c00279>.

Pose retrieval docking data for compound **4** in the crystal structure of PD-L1 (PDB code 5J80); pose retrieval docking data for compound **4** in the crystal structure of PD-L1 (PDB codes:5N2F,5NIU,5N2D,5NIX,5J89,6R3K); and superimposed cocrystallized and redocked poses of compound **4** at the PD-L1 dimer interface (PDF)

## ■ AUTHOR INFORMATION

### Corresponding Authors

**Hend M. El Tayebi** – Molecular Pharmacology Research Group, Department of Pharmacology and Toxicology, Faculty of Pharmacy and Biotechnology, German University in Cairo, 11835 Cairo, Egypt; Email: [Hend.saber@guc.edu.eg](mailto:Hend.saber@guc.edu.eg)

**Yasmine M. Mandour** – School of Life and Medical Sciences, University of Hertfordshire Hosted by Global Academic Foundation, 11578 Cairo, Egypt; Department of Pharmaceutical Chemistry, Faculty of Pharmacy and Biotechnology, German University in Cairo, 11835 Cairo, Egypt; [orcid.org/0000-0001-7104-3268](https://orcid.org/0000-0001-7104-3268); Email: [y.mandour@herts.ac.uk](mailto:y.mandour@herts.ac.uk), [yasminemandour@yahoo.com](mailto:yasminemandour@yahoo.com)

### Authors

**Monica A. Kamal** – Molecular Pharmacology Research Group, Department of Pharmacology and Toxicology, Faculty of Pharmacy and Biotechnology, German University in Cairo, 11835 Cairo, Egypt; [orcid.org/0000-0001-8578-8295](https://orcid.org/0000-0001-8578-8295)

**Hedy A. Badary** – Endemic Medicine and Hepato-gastroenterology Department, Faculty of Medicine, Cairo University, 11562 Cairo, Egypt; [orcid.org/0000-0003-3012-2204](https://orcid.org/0000-0003-3012-2204)

**Dalia Omran** – Endemic Medicine and Hepato-gastroenterology Department, Faculty of Medicine, Cairo University, 11562 Cairo, Egypt

**Hend I. Shousha** – Endemic Medicine and Hepato-gastroenterology Department, Faculty of Medicine, Cairo University, 11562 Cairo, Egypt

**Ashraf O. Abdelaziz** – Endemic Medicine and Hepato-gastroenterology Department, Faculty of Medicine, Cairo University, 11562 Cairo, Egypt

Complete contact information is available at: <https://pubs.acs.org/10.1021/acsomega.3c00279>

## Author Contributions

<sup>†</sup>M.A.K. and H.A.B. contributed equally to this paper.

## Notes

The authors declare no competing financial interest.

## ■ ACKNOWLEDGMENTS

The authors thank the Egyptian Academy of Scientific Research and Technology, grant number 90D/2021 for funding this work. The authors also thank Mariam El-Zohairy, a lecturer assistant at the Faculty of Pharmacy at the German University in Cairo, for her help in the modeling part of this work.

## ■ REFERENCES

- (1) Ishida, Y.; Agata, Y.; Shibahara, K.; Honjo, T. Induced Expression of PD-1, a Novel Member of the Immunoglobulin Gene Superfamily, upon Programmed Cell Death. *EMBO J.* **1992**, *11*, 3887–3895.
- (2) Ganesan, A.; Ahmed, M.; Okoye, I.; Arutyunova, E.; Babu, D.; Turnbull, W. L.; Kundu, J. K.; Shields, J.; Agopowicz, K. C.; Xu, L.; Tabana, Y.; Srivastava, N.; Zhang, G.; Moon, T. C.; Belovodskiy, A.; Hena, M.; Kandadai, A. S.; Hosseini, S. N.; Hitt, M.; Walker, J.; Smylie, M.; West, F. G.; Siraki, A. G.; Lemieux, M. J.; Elahi, S.; Nieman, J. A.; Tyrrell, D. L.; Houghton, M.; Barakat, K. Comprehensive In Vitro Characterization of PD-L1 Small Molecule Inhibitors. *Sci. Rep.* **2019**, *9*, 12392.
- (3) Lin, D. Y.; Tanaka, Y.; Iwasaki, M.; Gittis, A. G.; Su, H.-P.; Mikami, B.; Okazaki, T.; Honjo, T.; Minato, N.; Garboczi, D. N. The PD-1/PD-L1 Complex Resembles the Antigen-Binding Fv Domains of Antibodies and T Cell Receptors. *Proc. Natl. Acad. Sci. U.S.A.* **2008**, *105*, 3011–3016.
- (4) Zak, K. M.; Kitel, R.; Przetocka, S.; Golik, P.; Guzik, K.; Musielak, B.; DömLing, A.; Dubin, G.; Holak, T. A. Structure of the Complex of Human Programmed Death 1, PD-1, and Its Ligand PD-L1. *Structure* **2015**, *23*, 2341–2348.
- (5) Lazar-Molnar, E.; Yan, Q.; Cao, E.; Ramagopal, U.; Nathenson, S. G.; Almo, S. C. Crystal Structure of the Complex between Programmed Death-1 (PD-1) and Its Ligand PD-L2. *Proc. Natl. Acad. Sci. U.S.A.* **2008**, *105*, 10483–10488.
- (6) Chemnitz, J. M.; Parry, R. V.; Nichols, K. E.; June, C. H.; Riley, J. L. SHP-1 and SHP-2 Associate with Immunoreceptor Tyrosine-Based Switch Motif of Programmed Death 1 upon Primary Human T Cell Stimulation, but Only Receptor Ligation Prevents T Cell Activation. *J. Immunol.* **2004**, *173*, 945–954.
- (7) Fife, B. T.; Pauken, K. E. The role of the PD-1 pathway in autoimmunity and peripheral tolerance: The role of the PD-1 pathway in autoimmunity and peripheral tolerance. *Acad. Sci.* **2011**, *1217*, 45–59.
- (8) Francisco, L. M.; Sage, P. T.; Sharpe, A. H. The PD-1 Pathway in Tolerance and Autoimmunity. *Immunol. Rev.* **2010**, *236*, 219–242.
- (9) Dong, H.; Strome, S. E.; Salomao, D. R.; Tamura, H.; Hirano, F.; Flies, D. B.; Roche, P. C.; Lu, J.; Zhu, G.; Tamada, K.; Lennon, V. A.; Celis, E.; Chen, L. Tumor-Associated B7-H1 Promotes T-Cell Apoptosis: A Potential Mechanism of Immune Evasion. *Nat. Med.* **2002**, *8*, 793–800.
- (10) De Sousa Linhares, A.; Battin, C.; Jutz, S.; Leitner, J.; Hafner, C.; Tobias, J.; Wiedermann, U.; Kundi, M.; Zlabinger, G. J.; Grabmeier-Pfistershammer, K.; Steinberger, P. Therapeutic PD-L1 Antibodies Are More Effective than PD-1 Antibodies in Blocking PD-1/PD-L1 Signaling. *Sci. Rep.* **2019**, *9*, 11472.
- (11) Zak, K. M.; Grudnik, P.; Guzik, K.; Zieba, B. J.; Musielak, B.; DömLing, A.; Dubin, G.; Holak, T. A. Structural Basis for Small Molecule Targeting of the Programmed Death Ligand 1 (PD-L1). *Oncotarget* **2016**, *7*, 30323–30335.
- (12) Guzik, K.; Zak, K. M.; Grudnik, P.; Magiera, K.; Musielak, B.; Törner, R.; Skalniak, L.; DömLing, A.; Dubin, G.; Holak, T. A. Small-Molecule Inhibitors of the Programmed Cell Death-1/Programmed

Death-Ligand 1 (PD-1/PD-L1) Interaction via Transiently Induced Protein States and Dimerization of PD-L1. *J. Med. Chem.* **2017**, *60*, 5857–5867.

(13) Skalniak, L.; Zak, K. M.; Guzik, K.; Magiera, K.; Musielak, B.; Pachota, M.; Szalazek, B.; Kocik, J.; Grudnik, P.; Tomala, M.; Krzanik, S.; Pyrc, K.; DömLing, A.; Dubin, G.; Holak, T. A. Small-Molecule Inhibitors of PD-1/PD-L1 Immune Checkpoint Alleviate the PD-L1-Induced Exhaustion of T-Cells. *Oncotarget* **2017**, *8*, 72167–72181.

(14) Gao, Y.; Wang, H.; Shen, L.; Xu, H.; Deng, M.; Cheng, M.; Wang, J. Discovery of Benzo[d]isothiazole Derivatives as Novel Scaffold Inhibitors Targeting the Programmed Cell Death-1/Programmed Cell Death-Ligand 1 (PD-1/PD-L1) Interaction through “Ring Fusion” Strategy. *Bioorg. Chem.* **2022**, *123*, 105769.

(15) Wang, Y.; Huang, K.; Gao, Y.; Yuan, D.; Ling, L.; Liu, J.; Wu, S.; Chen, R.; Li, H.; Xiong, Y.; Liu, H.; Ma, J. Discovery of Quinazoline Derivatives as Novel Small-Molecule Inhibitors Targeting the Programmed Cell Death-1/Programmed Cell Death-Ligand 1 (PD-1/PD-L1) Interaction. *Eur. J. Med. Chem.* **2022**, *229*, 113998.

(16) Tianjin Chasesun Pharmaceutical Co., LTD. A Phase I Clinical Trial of IMM-010 in Patients With Advanced Malignant Solid Tumors. <https://www.clinicaltrials.gov/ct2/show/NCT04343859> (accessed March 6, 2023).

(17) Maxinovel Pty., Ltd. A Phase I Study of MAX-10181 Given Orally to Patients With Advanced Solid Tumor. <https://www.clinicaltrials.gov/ct2/show/NCT04122339> (accessed March 6, 2023).

(18) Specs - Compound Management services and Research Compounds for the Life Science industry. <https://www.specs.net/> (accessed February 9, 2022).

(19) Broby, D.; Sahota, A.; Zhang, B. System for Estimating Value of Company Using Financial Technology. U.S. Patent 16,263,582; Uniw. śląski, 2019.

(20) Bondarev, D. Align\_all.svl, CCG SVL Exchange, 2017. <https://svl.chemcomp.com/> (accessed September 10, 2022).

(21) *Molecular Operating Environment (MOE)*, 2022.02 Chemical Computing Group ULC, 1010 Sherbooke St. West, Suite #910, Montreal, QC, Canada, H3A 2R7, 2022.

(22) US Patent Application for COMPOUNDS USEFUL AS IMMUNOMODULATORS Patent Application (Application #20180057455 issued March 1, 2018) - Justia Patents Search. <https://patents.justia.com/patent/20180057455> (accessed February 9, 2022).

(23) USPTO.report. Compounds Useful as Immunomodulators Patent Application <https://uspto.report/patent/app/20150291549> (accessed February 9, 2022).

(24) Vogel, S. M.; Bauer, M. R.; Boeckler, F. M. DEKOIS: demanding evaluation kits for objective in silico screening—a versatile tool for benchmarking docking programs and scoring functions. *J. Chem. Inf. Model.* **2011**, *51*, 2650–2665.

(25) Erbe, D. V.; Wang, S.; Xing, Y.; Tobin, J. F. Small Molecule Ligands Define a Binding Site on the Immune Regulatory Protein B7.1. *J. Biol. Chem.* **2002**, *277*, 7363–7368.

(26) Mysinger, M. M.; Carchia, M.; Irwin, J. J.; Shoichet, B. K. Directory of Useful Decoys, Enhanced (DUD-E): Better Ligands and Decoys for Better Benchmarking. *J. Med. Chem.* **2012**, *55*, 6582–6594.

(27) Jones, G.; Willett, P.; Glen, R. C.; Leach, A. R.; Taylor, R. Development and Validation of a Genetic Algorithm for Flexible Docking 1 Edited by F. E. Cohen. *J. Mol. Biol.* **1997**, *267*, 727–748.

(28) Neudert, G.; Klebe, G. DSX: A Knowledge-Based Scoring Function for the Assessment of Protein–Ligand Complexes. *J. Chem. Inf. Model.* **2011**, *51*, 2731–2745.

(29) Sunseri, J.; Koes, D. R. Pharmit: Interactive Exploration of Chemical Space. *Nucleic Acids Res.* **2016**, *44*, W442–W448.

(30) Zhan, M. M.; Hu, X. Q.; Liu, X. X.; Ruan, B. F.; Xu, J.; Liao, C. From Monoclonal Antibodies to Small Molecules: The Development of Inhibitors Targeting the PD-1/PD-L1 Pathway. *Drug Discovery Today* **2016**, *21*, 1027–1036.

(31) Shaabani, S.; Huizinga, H. P. S.; Butera, R.; Kouchi, A.; Guzik, K.; Magiera-Mularz, K.; Holak, T. A.; DömLing, A. A Patent Review on PD-1/PD-L1 Antagonists: Small Molecules, Peptides, and Macrocycles (2015–2018). *Expert Opin. Ther. Pat.* **2018**, *28*, 665–678.

(32) Zarganes-Tzitzikas, T.; Konstantinidou, M.; Gao, Y.; Krzemien, D.; Zak, K.; Dubin, G.; Holak, T. A.; DömLing, A. *Inhibitors of Programmed Cell Death 1 (PD-1): A Patent Review (2010–2015)*, 2016; Vol. 26, pp 973–977. DOI: 10.1080/13543776.2016.1206527.

(33) Kamal, M. A.; Mandour, Y. M.; Abd El-Aziz, M. K.; Stein, U.; El Tayebi, H. M. Small Molecule Inhibitors for Hepatocellular Carcinoma: Advances and Challenges. *Molecules* **2022**, *27*, 5537.

(34) Wang, M.; Zhai, X.; Li, J.; Guan, J.; Xu, S.; Li, Y. Y.; Zhu, H. The Role of Cytokines in Predicting the Response and Adverse Events Related to Immune Checkpoint Inhibitors. *Front. Immunol.* **2021**, *12*, 12.

(35) Zhao, N.; Yi, Y.; Cao, W.; Mei, N.; Fu, X.; Li, C. Serum Cytokine Levels for Predicting Immune-Related Adverse Events and the Clinical Response in Lung Cancer Treated with Immunotherapy. *Front. Oncol.* **2022**, *12*, 923531.

(36) El-Zohairy, M. A.; Zlotos, D. P.; Berger, M. R.; Adwan, H. H.; Mandour, Y. M. Discovery of Novel CCR5 Ligands as Anticancer Agents by Sequential Virtual Screening. *ACS Omega* **2021**, *6*, 10921–10935.

(37) The PyMOL Molecular Graphics System, version 1.8; Schrödinger, LLC. <http://www.sciencedirect.com/reference/159710> (accessed September 10, 2022).

(38) Case, D. A.; Cheatham, T. E.; Darden, T.; Gohlke, H.; Luo, R.; Merz, K. M.; Onufriev, A.; Simmerling, C.; Wang, B.; Woods, R. J. The Amber Biomolecular Simulation Programs. *J. Comput. Chem.* **2005**, *26*, 1668–1688.

(39) Mandour, Y. M.; Zlotos, D. P.; Alaraby Salem, M. A Multi-Stage Virtual Screening of FDA-Approved Drugs Reveals Potential Inhibitors of SARS-CoV-2 Main Protease. *J. Biomol. Struct. Dyn.* **2022**, *40*, 2327–2338.

(40) Toumi, A.; Boudriga, S.; Mandour, Y. M.; Mekki, A. A.; Knorr, M.; Strohmman, C.; Kirchhoff, J. L.; Sobeh, M. Design of Novel Enantiopure Dispirooxindolopyrrolidine-Piperidones as Promising Candidates toward COVID-19: Asymmetric Synthesis, Crystal Structure and In Silico Studies. *Molecules* **2022**, *27*, 3945.

(41) Roe, D. R.; Cheatham, T. E. PTRAJ and CPPTRAJ: Software for Processing and Analysis of Molecular Dynamics Trajectory Data. *J. Chem. Theory Comput.* **2013**, *9*, 3084–3095.

(42) Soman, S. S.; Sivakumar, K. C.; Sreekumar, E. Molecular dynamics simulation studies and in vitro site directed mutagenesis of avian beta-defensin Apl\_AvBD2. *Bioinformatics* **2010**, *11*, S7.

(43) Humphrey, W.; Dalke, A.; Schulten, K. VMD: Visual Molecular Dynamics. *J. Mol. Graphics* **1996**, *14*, 33–38.

(44) Loncharich, R. J.; Brooks, B. R.; Pastor, R. W. Langevin Dynamics of Peptides: The Frictional Dependence of Isomerization Rates of N-Acetylalanyl-N'-Methylamide. *Biopolymers* **1992**, *32*, 523–535.

(45) Darden, T.; York, D.; Pedersen, L. Particle Mesh Ewald: An N log(N) Method for Ewald Sums in Large Systems. *J. Chem. Phys.* **1993**, *98*, 10089–10092.

(46) Genheden, S.; Ryde, U. The MM/PBSA and MM/GBSA Methods to Estimate Ligand-Binding Affinities. *Expert Opin. Drug Discovery* **2015**, *10*, 449–461.